

Large-eddy simulation of accelerating boundary layers

Giuseppe De Prisco*, Anthony Keating † and Ugo Piomelli ‡

Department of Mechanical Engineering, University of Maryland, College Park, MD, 20740, USA

Large-eddy simulation of flat-plate boundary layers in favorable pressure gradients (FPG) are performed for two different acceleration parameters. The high-acceleration case is in good agreement with the experimental data by Fernholz and Warnack. Substantial reduction in turbulent kinetic energy, strong decorrelation of u and v fluctuation, and a reduction of the bursting frequency indicate that the accelerated boundary layer is in a laminar-like state when the pressure-gradient parameter K exceeds a threshold value. Downstream of this region, the boundary layer has a fast re-transition to turbulence: it seems due to the turbulent structures present in the outer part of the boundary layer. In the low K case, the boundary layer does not depart significantly from equilibrium.

I. Introduction

Turbulent boundary layers subjected to a favorable pressure gradient (FPG) (*i.e.*, one that results in freestream acceleration) are common in many engineering applications, such as airfoils and curved ducts. While the canonical zero-pressure-gradient (ZPG) boundary layer is relatively well understood, FPG boundary-layers are less well known. The simplest case of an accelerating boundary layer is the “sink flow”, in which the acceleration parameter $K = (\nu/U_\infty^2)dU_\infty/dx$ is constant with the streamwise distance x . This flow has been studied experimentally and numerically; it is known that, for strong acceleration ($K > 3 \times 10^{-6}$) turbulence cannot be maintained, and the flow re-laminarizes. The sink flow is, of course, an idealization: in real cases, a large acceleration parameter cannot be sustained for long distances, and, in practical applications, a region of FPG and streamwise acceleration, is followed by one with constant or adverse pressure gradient (such is the case for the flow on an airfoil downstream of maximum thickness). In these conditions, full re-laminarization may not occur, and the pressure gradient may leave the flow in a “laminar-like”¹ state. As the pressure gradient is removed, the flow may then return to a turbulent state; the re-transitioning process may be strongly affected by the state of the turbulence at the end of the acceleration region.

For these reasons it is important to understand the mechanisms of re-laminarization. Reviews of current knowledge can be found in several articles by Narasimha and Sreenivasan^{2,3} and by Sreenivasan;¹ here, only the main findings are summarized. Re-laminarization can be caused by three mechanisms: (1) a decrease in the Reynolds number accompanied by an increase in the viscous dissipation; (2) stratification or flow curvature, or (3) flow acceleration. Experimental investigations of re-laminarization due to flow acceleration started in the early 1960s. Wilson⁴ found the first evidence that the flow did not follow the semi-empirical theories for a fully turbulent boundary layer: the measured heat-flux rates on a convex surface of a blade were considerably lower than the predicted values. Wilson⁴ conjectured the possibility of a “reverse transition” of the flow due to the low local value of the Reynolds number. However, Patel and Head⁵ later observed that there is no explicit correlation between a low Re and the relaminarization process, as long as the initial Re is high enough to allow the turbulence to be self-sustained.

Senoo⁶ studied the boundary layer on the end-wall of a turbine nozzle cascade; he found that the boundary layer was laminar in the region of the throat were the upstream layer was turbulent. His findings did not explain the phenomenon of relaminarization. Moreover, the effects of secondary flow were not clear in his study.

*PhD Student, AIAA Student-Member.

†Present Address: Exa Corporation, Burlington, MA 01803, USA

‡Professor, AIAA Associate Fellow

Copyright © 2007 by the American Institute of Aeronautics and Astronautics, Inc. All rights reserved.

Studying a similar configuration, Launder^{7,8} observed that relaminarization of the flow, at least in terms of macro-scale properties and integral parameters, starts near the end of the acceleration region. In the upstream region, the boundary layer was found to be turbulent but with a departure from the universal law of the wall. Only later the boundary layer became close to the laminar state. Moreover, he documented an increase of the energy at low wave-numbers in the near-wall region and an even more pronounced one in the outer part of the boundary layer. He found an explanation of that energy shift in the time-lag between inner and outer regions: the latter is relatively distant from the turbulence production peak, so the eddies in that region are not fast enough to adjust their frequency as the free stream is accelerated. He, therefore, proposes a picture in which the flow dynamics are completely dominated by the near wall region. Launder^{7,8} also observed that the turbulence does not vanish, but an increasing fraction of it plays a passive role in the boundary-layer development. Because of this inability of turbulent structures to adjust to the flow acceleration and the rapid increase of momentum, the viscous stresses grow larger than the turbulent ones; consequently, the dissipation exceeds production, leading to a decay of turbulence and to laminarization. However, Badri-Narayan *et al.*⁹ found that dissipation never exceeds production in an accelerated boundary layer, and that both production and dissipation decrease.

Kline *et al.*¹⁰ found a correlation between the drastic drop of eruptions in the buffer layer and the acceleration parameter K : for K that approach the value of $K_{\max} \approx 3.5 \times 10^{-6}$ the burst rate tended to zero. Narasimha and Sreenivasan³ suggested that the bursting frequency decreases exponentially in an accelerated boundary layer before the flow relaminarizes, but never goes to zero completely.

Patel and Head⁵ showed a strong correlation between the distribution of the shear-stress gradient near the wall and the relaminarization. They defined a non-dimensional shear-stress-gradient parameter, and they inferred the onset of relaminarization from the position where this parameter has a minimum value of -0.009 . However, Narasimha and Sreenivasan³ observed that this non-dimensional parameter reaches that value before the turbulent boundary-layer actually reverts to a laminar-like state; in this sense, the Patel and Head⁵ parameter predicts deviation from the universal law for ZPG boundary layers, but not necessarily relaminarization.

Blackwelder and Kovasznay¹¹ noted an increase of the Reynolds stress and turbulent kinetic energy (TKE) along streamlines in the outer part of the boundary layer as the flow was accelerated. In the inner layer, on the other hand, they found a decrease of those quantities along streamlines. Moreover, they studied the space-time correlations of the large structure in the outer layer. They found no change compared to the ZPG case for the uu correlations; this suggested that the acceleration had no strong effect on the large streamwise structure (those close to the boundary-layer edge). On the other hand, they noted a drastic change of the normal velocity component of the outer-layer structures, as the vv correlations lost the anti-symmetrical part found in the ZPG case.

Narasimha and Sreenivasan² point out that relaminarization is the result of the domination of pressure forces over the slowly responding Reynolds stresses in the outer layer, and the generation of a new laminar sub-layer that is maintained stable by the acceleration. In their model the turbulent structures in the outer layer are only distorted and not destroyed by the rapid acceleration. The new sub-layer and the distorted outer layer do not interact, but they only provide the appropriate boundary conditions. Rapid distortion theory could be applied in the outer part to predict the turbulence intensities there, but the interior part of the layer was not well understood and the wall-normal components were not well predicted. In the same period, Falco¹² performed a smoke-visualization study, and suggested that in the relaminarization process large scale structures existed upstream of the contraction that accelerates the flow: the boundary layer in the later stages of the acceleration is dominated by an array of large scale streamwise vortices; thus, an inner-outer layer interaction could exist and the relaminarization seems to begin from the outer region with a strong coupling between inner and outer parts. This visual observation was reconfirmed by Ichimiya *et al.*,¹³ who conjecture that non-turbulent fluid on the outside of the boundary layer penetrates near the wall, so that the beginning of relaminarization is due to the outer region together with the change in ejection-sweep phenomena.

Recent experimental studies of FPG boundary layers have been performed by Fernholz and Warnack¹⁴ and by Warnack and Fernholz.¹⁵ Their measurements showed that the Reynolds number had little effect on the relaminarization, and the pressure-gradient effects were dominant. They found a strong increase in the anisotropy of the normal Reynolds stresses (which decreased) in the outer region of the boundary layer, but observed the opposite effect in the inner layer. By calculating the integral length-scales, they found that the near-wall vortices are stretched in the streamwise direction, but are only slightly smaller in the wall-normal

direction. They measured high levels of flatness of the instantaneous skin friction coefficient, which indicated the presence of intermittent high-frequency bursts in the re-laminarizing flow.

Other recent experiments by Escudier *et al.*¹⁶ found that the streamwise RMS velocity in the inner layer scales with the local freestream velocity, while in the outer layer it is “frozen” (*i.e.*, remains relatively constant) in the accelerated region. They inferred that the frequency content of the turbulence was only changed at the highest frequencies, and that the bulk of the turbulence generated in the thick upstream boundary layer prior to acceleration was at frequencies too low to cause significant Reynolds stresses within the accelerated boundary-layer.

Numerical calculations of a boundary layer with variable acceleration parameters (as opposed to the sink flow studied by Spalart¹⁷) were carried out by Piomelli *et al.*,¹⁸ who examined the effect of the acceleration on the near-wall vortical structures. They observed that the near-wall streaks became more elongated and showed fewer undulations. Since they found that the vorticity levels in the acceleration region were similar to those in the zero-pressure gradient (ZPG) boundary-layer, and that the vortex scales in the cross-plane were unchanged, they suggested that the additional vortex-stretching due to the streamwise velocity gradient must be counterbalanced by other mechanisms. However, from the results presented, it was unclear which physical phenomena provide this balance.

The mechanisms involved in the relaminarization of the turbulent boundary layer in an FPG are still relatively unknown. What is clear, however, is that the turbulence in the outer layer remains frozen through the acceleration, and is, therefore, strongly dependent on the conditions of the upstream boundary layer (*i.e.*, neither on the local near-wall behavior nor on the local freestream velocity). Closer to the wall, the flow undergoes a process of laminarization, in which the skin friction coefficient drops sharply. Finally, after the acceleration is completed, the flow quickly re-transitions to an equilibrium boundary layer. Several questions are still open; among them are: (1) Is the outer layer turbulence frozen or is the main actor in the relaminarization phenomenon? (2) How do the inner and outer layers interact during and after the acceleration? (3) How does the re-transition to turbulence takes place (and why it takes place so abruptly)?

In an attempt to clarify at least the first of these points, large-eddy simulations (LES) of boundary layers in FPG are performed with different acceleration parameters. The first simulation, which matches the high-acceleration experiment of Warnack and Fernholz¹⁵ ($K_{\max} \approx 4 \times 10^{-6}$) (where $K = (\nu/U_\infty^2)(dU_\infty/dx)$ is the acceleration parameter), shows a substantial reduction in turbulent kinetic energy production, and the flow becomes laminar-like in the acceleration region. A second simulation is performed at a lower acceleration ($K_{\max} \approx 3 \times 10^{-6}$) (obtained by scaling down the high- K case) resulting in less of a “laminar-like” behavior in the acceleration (for comparison, on a 0.3m-long NACA0012 airfoil at $Re = 1.5 \times 10^6$, K has values of the order 3×10^{-6} in the region between 2% of the chord and the point of maximum thickness).

In the following we will present the numerical approach employed. Then will show results of the simulations, including statistics and flow visualizations; we will describe the results of some numerical experiments in which the flow was artificially altered, to isolate the structures responsible for the re-transition. Finally, we shall draw some conclusions.

II. Problem formulation

In this study we perform large-eddy simulations (LES) of a flat-plate boundary layer in the presence of an accelerating freestream. The governing equations are the incompressible filtered Navier-Stokes equations (made dimensionless using a reference length, δ_o^* and velocity U_o), which can be written as

$$\frac{\partial \bar{u}_i}{\partial x_i} = 0 \tag{1}$$

$$\frac{\partial \bar{u}_i}{\partial t} + \frac{\partial \bar{u}_j \bar{u}_i}{\partial x_j} = \frac{1}{Re} \frac{\partial^2 \bar{u}_i}{\partial x_j \partial x_j} - \frac{\partial \bar{p}}{\partial x_i} - \frac{\partial \tau_{ij}}{\partial x_j} \tag{2}$$

Here, x , y and z are the streamwise, wall-normal and spanwise directions, and u , v , and w (or u_1 , u_2 and u_3) are the velocity components in the three coordinate directions. The subgrid-scale stresses

$$\tau_{ij} = \overline{u_i u_j} - \bar{u}_i \bar{u}_j \tag{3}$$

were parametrized using the dynamic eddy-viscosity subgrid-scale model^{19,20} with the eddy-viscosity coefficient averaged over Lagrangian flow pathlines.²¹

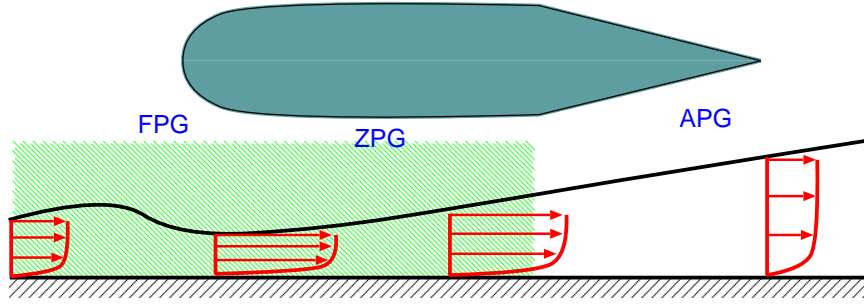


Figure 1. Sketch of the configuration. The computational domain is shown as a hatched area.

Most experimental measurements in FPG boundary layer are performed on a flat surface in which the pressure gradient is imposed through contouring of the opposite wall of the wind-tunnel, or by including a contoured body above the flat wall to produce the desired acceleration (Figure 1). In our case we imposed directly a variable freestream velocity^a $U_\infty(x)$ on the top boundary of the domain.²² The other two velocity components were obtained by requiring that the vorticity in the freestream is zero. An unsteady inflow boundary condition was obtained from a separate simulation that used the recycling/rescaling method,²² while a convective outflow boundary condition was used at the downstream boundary.²³ Periodic conditions were used in the spanwise direction.

The simulations were performed on a domain of size $476\delta_o^* \times 20\delta_o^* \times 20\delta_o^*$ (in the streamwise, wall-normal and spanwise directions, respectively), using $1136 \times 104 \times 192$ grid points for the high-acceleration case, and $1024 \times 64 \times 128$ grid points for the low-acceleration one. The results obtained using this resolution compare well with coarser calculations. The Reynolds number, based on freestream velocity at the inflow, U_o , and on the displacement thickness at the inflow, δ_o^* , is 1,260.

Equations (1–2) were solved on a Cartesian staggered grid. Conservative second-order finite differences were used for spatial discretization while a semi-implicit fractional-step method^{24,25} was used for time integration. The equations of motion were integrated for $3171\delta_o^*/U_o$ time units. Statistical data were obtained by averaging over the last 2415 time units, and over the spanwise direction. In the following, time-averaged quantities are denoted by angle brackets, and fluctuating ones by a prime.

III. Results

In the present investigation we studied two cases: one with high-acceleration, another with lower acceleration. Figure 2(a) shows the freestream velocity, U_∞/U_o , and the resulting friction velocity $u_\tau/u_{\tau,o}$ for the two cases of high and low acceleration. Figure 2(b) shows the acceleration parameter, K . In the case of high K , the freestream velocity at the outflow is almost three times that at the inflow.

The momentum-thickness Reynolds number $Re_\theta = U_\infty\theta/\nu$, with

$$\theta = \int_0^\infty \frac{U}{U_\infty} \left(1 - \frac{U}{U_\infty}\right) dy \quad (4)$$

(where $U = \langle \bar{u} \rangle$) is shown in Figure 2(c); Re_θ decreases as the flow begins to accelerate ($x/\delta_o^* > 140$). This reflects profound changes in the velocity profile, which result in significant decrease of θ and will be discussed further later. The skin-friction coefficient,

$$C_f = \frac{\tau_w}{\rho U_\infty^2/2} \quad (5)$$

is shown in Figure 2(d). Again, it can be observed that, although the mean freestream velocity increases in both cases, C_f begins to decrease near the location of maximum K (this decrease begins to occur downstream of the corresponding decrease in Re_θ). After the pressure gradient is relaxed, rapid re-transition towards an equilibrium turbulent value occurs ($x/\delta_o^* \simeq 310$). The chain-dotted line shows the equilibrium ZPG value of C_f obtained from the correlation²⁶ $C_f = 0.0576Re_x^{-0.2}$. At the inflow, while the computations show good agreement with the experimental correlation, the experiments have lower skin friction, suggesting

^aIn the following, U_∞ denotes the (variable) freestream velocity, whereas $U_o = U_\infty(0) = 1$ is the reference velocity for the flat-plate region upstream of the FPG region.

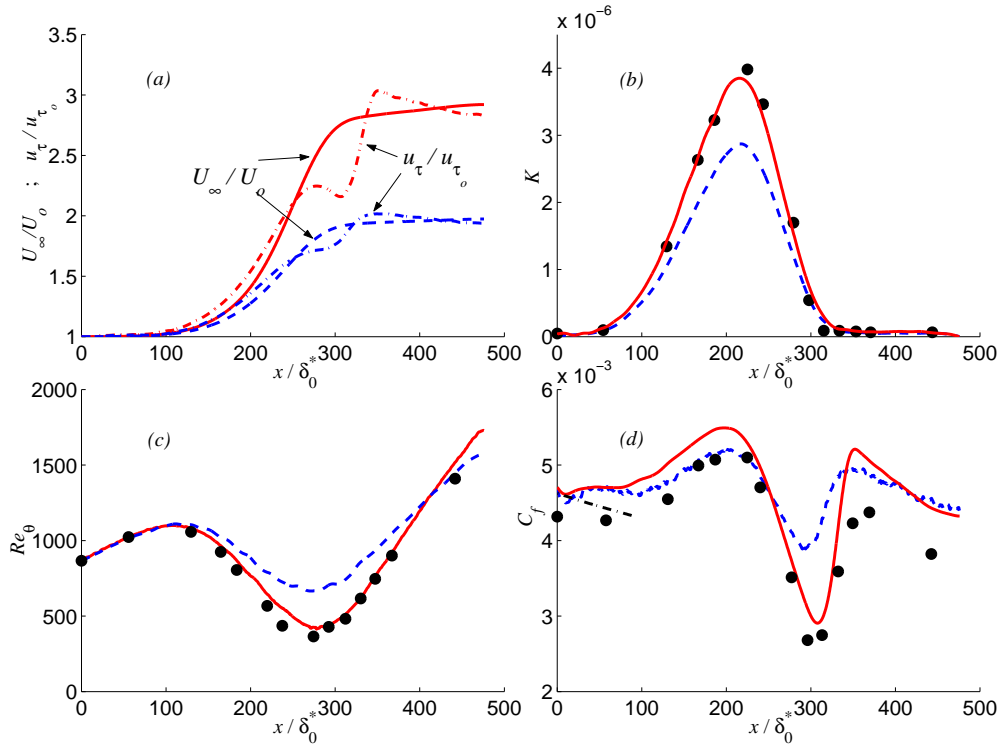


Figure 2. Streamwise development of statistical quantities. (a) Freestream velocity, U_∞/U_0 and friction velocity u_τ/u_{τ_0} ; (b) Acceleration parameter K ; (c) Momentum-thickness Reynolds number Re_θ ; (d) Skin friction coefficient C_f . • Experiments;¹⁴ — high- K case; - - low- K case; - - ZPG boundary-layer correlation.

that pressure gradient effects are already significant on the upstream boundary layer. The region of relaminarization is predicted well by the LES. The re-transitioning occurs more abruptly than in the experiment, and the downstream C_f is higher in the LES, even taking into account the initial shift. Several factors can account for this difference. First, the different geometry: in the experiment the measurements are made on the inside wall of a cylinder, whereas the calculation uses a flat plate;¹² the ratio between cylinder radius and boundary-layer thickness varies between 12 and 9, so curvature effects may play a role. Furthermore, despite the fact that the grid in the streamwise direction was refined in the re-transition region, the three-fold increase in the friction velocity results in marginal resolution of the boundary layer in the fully turbulent region downstream of the acceleration: in the upstream region we have $\Delta x^+ \simeq 28$, $\Delta z^+ \simeq 6.2$, while in the recovery region $\Delta x^+ \simeq 56$ and $\Delta z^+ \simeq 19$.

The lower acceleration case shows similar behavior to the high-acceleration one; however the relaminarization is less severe. Re_θ and C_f are reduced by a much smaller amount, U_∞ in the acceleration region, and recovery takes place earlier than for the high- K case.

Figure 3 shows the mean velocity profiles in outer coordinates at several locations in the flow. If the velocity profiles are plotted in wall coordinates (Figure 4), one can observe the existence of a logarithmic layer (following the standard law, $U^+ = 2.5 \log y^+ + 5$) at the inflow and in the mild acceleration region ($x/\delta_0^* < 150$). As the FPG becomes significant, the slope of the logarithmic region decreases (a well-known effect of acceleration¹⁷). The two cases are in good agreement up to the point of maximum K . Thereafter, the high- K case departs significantly from the equilibrium boundary layer profile, becoming more laminar-like. The recovery of the inner layer to an equilibrium logarithmic law occurs quite rapidly, between $x/\delta_0^* \simeq 330$ and 370. The agreement with the experimental data is very good. One should observe that in the region of high acceleration there is a significant region of well-mixed fluid, in which the normal velocity gradient is nearly zero (from $y/\theta > 5$ at $x/\delta_0^* = 320$, for instance).

Very good agreement is also observed in the prediction of the normal Reynolds stresses (Figure 5). The decrease of the magnitude of the stresses following the maximum of the acceleration is evident, and is due to the increase of u_τ^2 , which is used to normalize the stresses, rather than to a decrease of the stresses themselves, which remain approximately equal to their upstream value (see the discussion below).

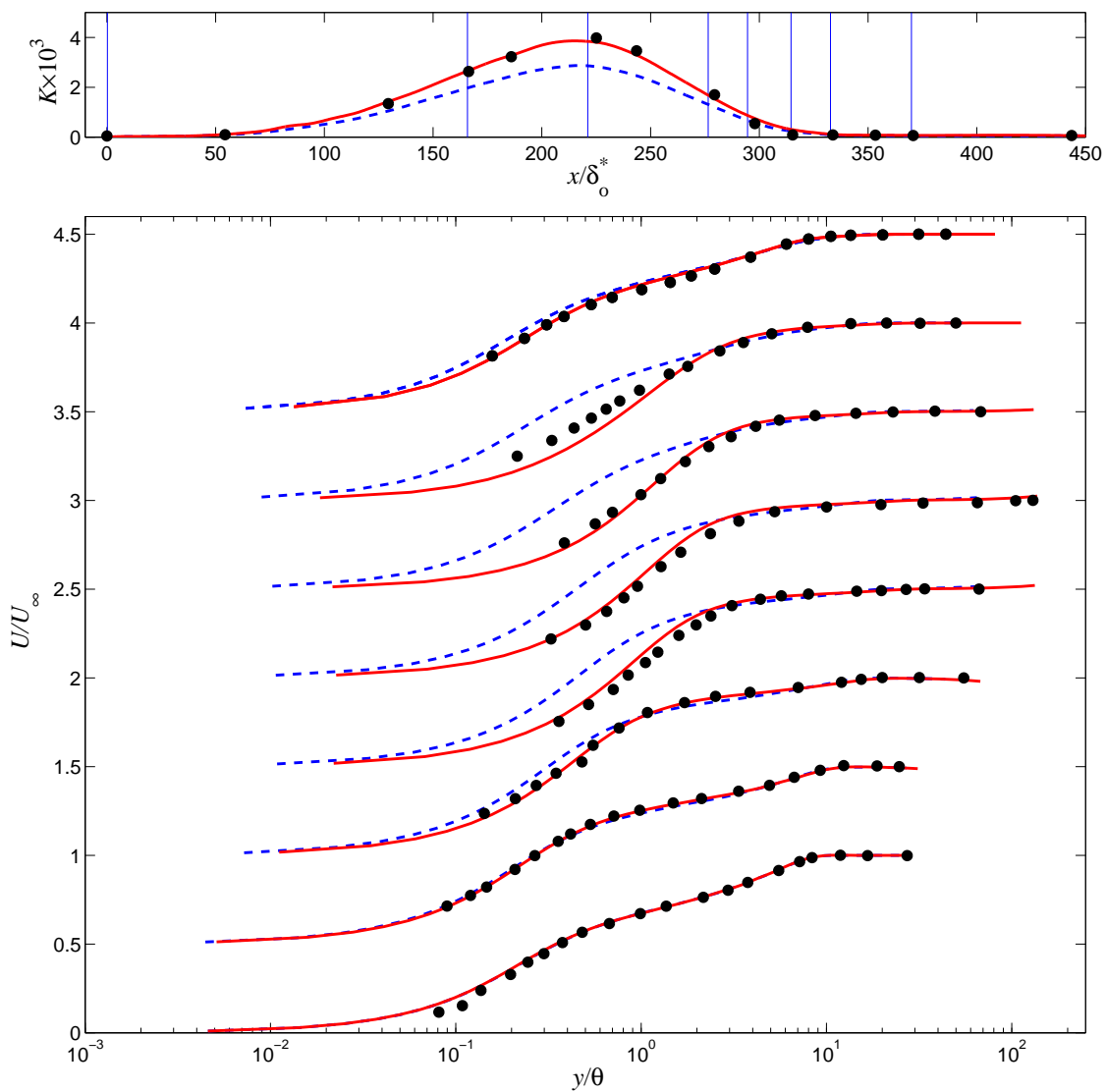


Figure 3. Wall-normal profiles of the mean streamwise velocity at the locations shown in the top figure. • Experiments;¹⁴
 — high- K case; - - low- K case.

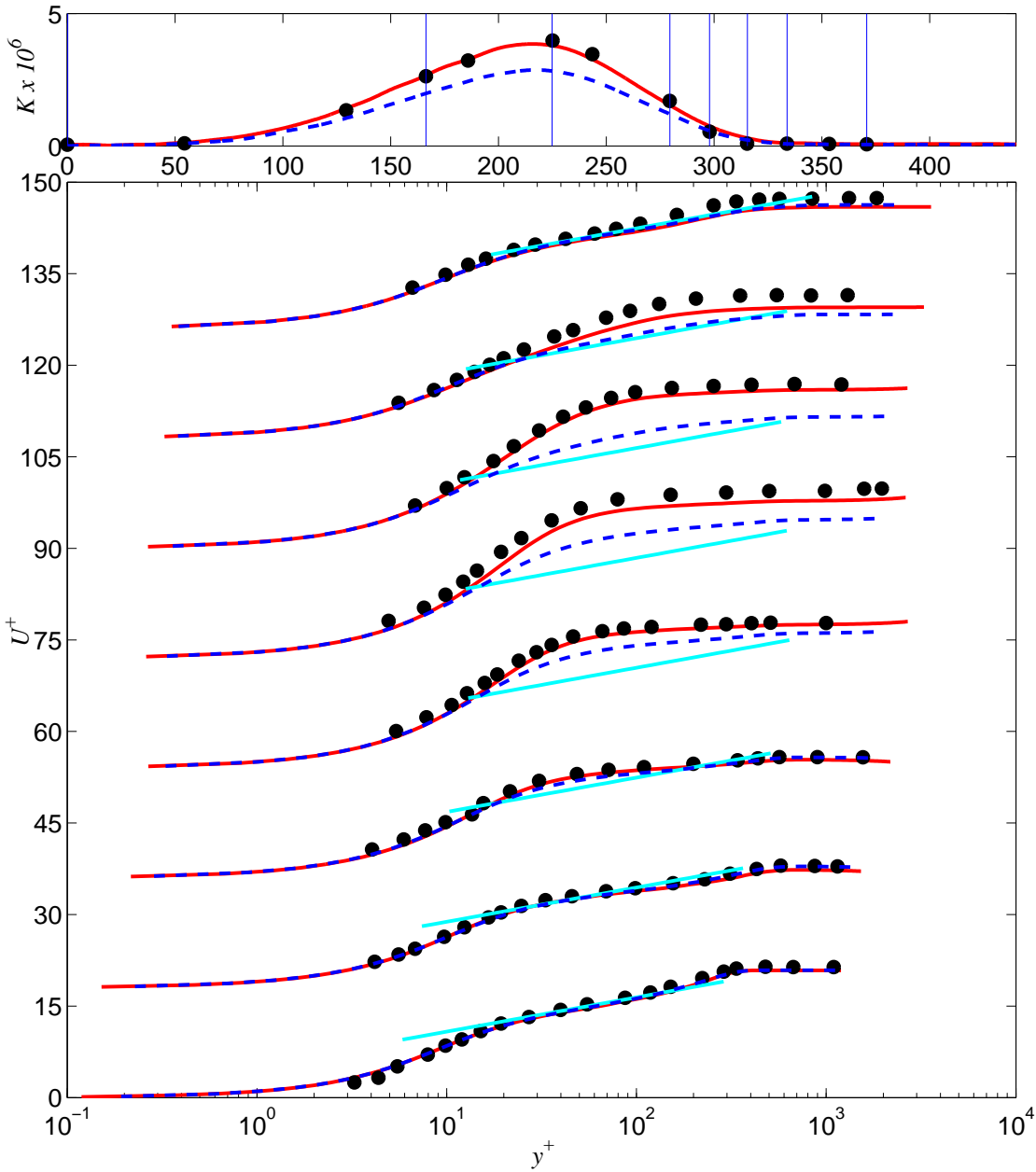


Figure 4. Wall-normal profiles of the mean streamwise velocity in inner coordinates at the locations shown in the top figure. • Experiments;¹⁴ — high- K case; - - low- K case; — $U^+ = 2.5 \log y^+ + 5$.

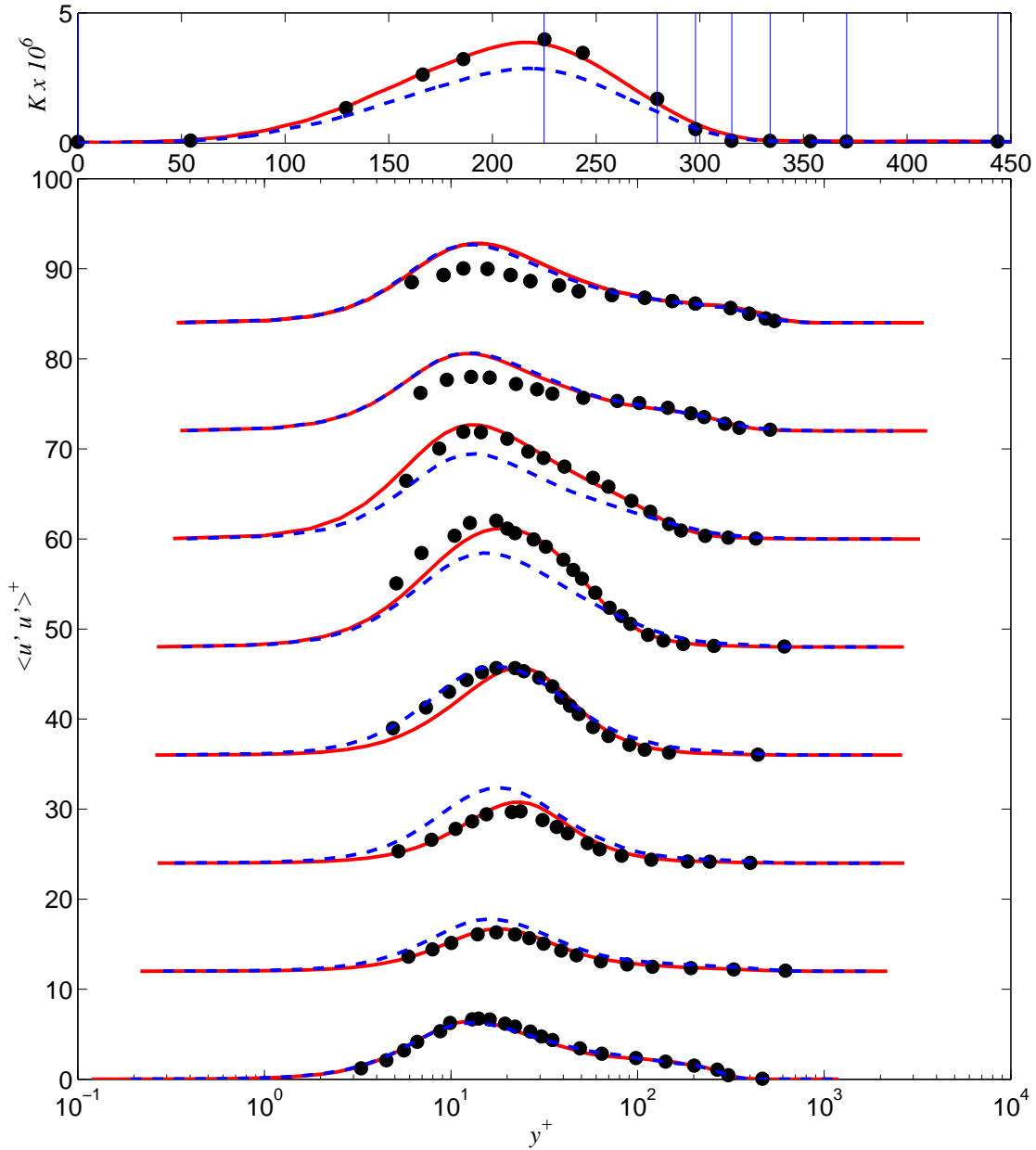


Figure 5. Wall-normal profiles of the streamwise Reynolds stresses at the locations shown in the top figure.
 • Experiments;¹⁴ — high- K case; - - low- K case.

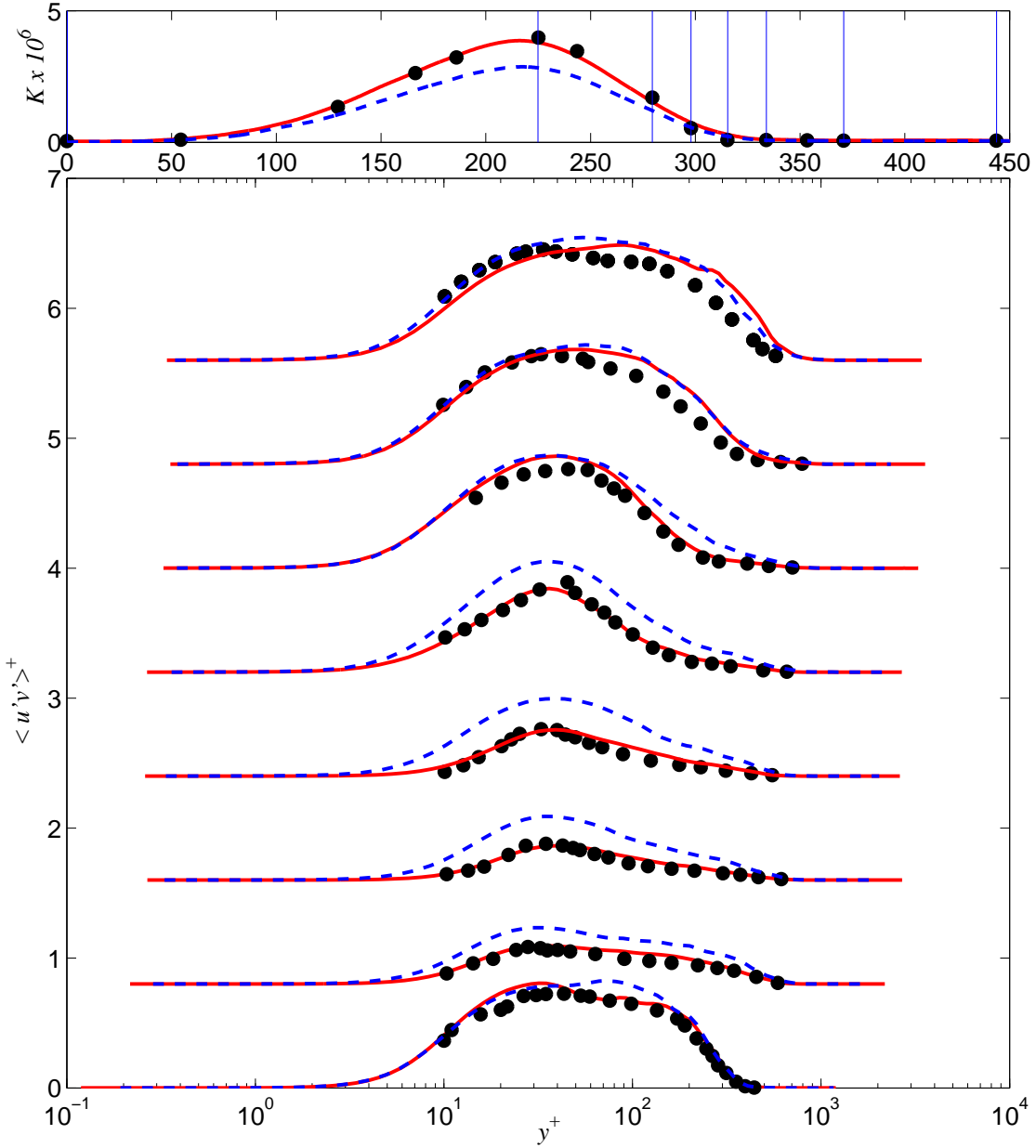


Figure 6. Wall-normal profiles of the Reynolds shear stresses at the locations shown in the top figure. • Experiments;¹⁴
 — high- K case; - - low- K case.

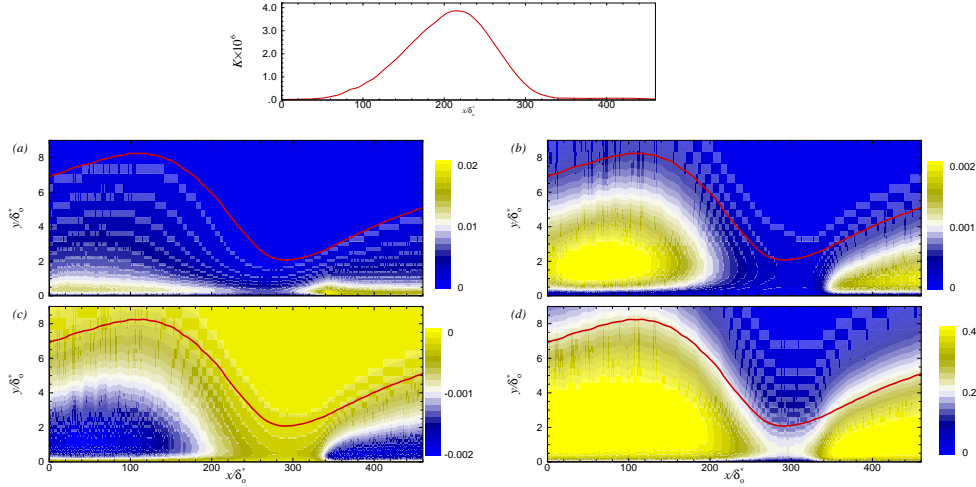


Figure 7. Contours of averaged quantities for the high- K case. The red line shows the local boundary layer thickness δ_{99} . (a) $\langle u'u' \rangle / U_\infty^2$; (b) $\langle v'v' \rangle / U_\infty^2$; (c) $\langle u'v' \rangle / U_\infty^2$; (d) $C_{uv} = \langle u'v' \rangle / u_{rms} v_{rms}$.

Figure 6 shows the Reynolds stresses in inner units; again, there is very good agreement with the experimental results. The Reynolds stresses decrease significantly in the region where K has the maximum value. In many cases flow relaminarization is due to decorrelation between the wall-normal and the streamwise fluctuations: both remain significant but do not contribute to the Reynolds shear stress. In this flow, the cause of the decrease of $\langle u'v' \rangle$ appears to be different. Figure 7 shows contours of the normal Reynolds stresses $\langle u'u' \rangle$ and $\langle v'v' \rangle$, of the shear stresses $\langle u'v' \rangle$, and of the correlation coefficient

$$C_{uv} = \frac{\langle u'v' \rangle}{(\langle u'u' \rangle \langle v'v' \rangle)^{1/2}} = \frac{\langle u'v' \rangle}{u_{rms} v_{rms}}. \quad (6)$$

From this figure it appear that, while the correlation coefficient decreases significantly around $x/\delta_o^* \simeq 300$, the decrease of the v' fluctuations is much more dramatic.

The same phenomenon is better illustrated in Figure 8. Here, we identified four streamlines (one in the outer layer, two in the logarithmic region and one in the buffer layer), and plot the streamwise development of the Reynolds stresses along each streamline. This method allows one to account for the significant thinning of the boundary layer in the high-acceleration region, and for its subsequent thickening in the re-transition region.

Focusing our attention first on the streamwise stresses, $\langle u'u' \rangle / U_o^2$ (Figure 8(b)), we observe that in the outer layer their level is essentially frozen (*i.e.*, they remain constant and equal to their upstream value) until a location well after the maximum acceleration point ($x/\delta_o^* \simeq 300$). They then begin to increase, an increase that occurs later for the streamline located farther away from the wall. Along the streamline in the buffer layer the increase in $\langle u'u' \rangle / U_o^2$ begins earlier, as soon as the freestream velocity begins to increase ($x/\delta_o^* \simeq 120$). A different behavior can be observed for the wall-normal stresses $\langle v'v' \rangle / U_o^2$ (Figure 8(c)): along the outer-layer streamlines the stresses also appear to be frozen to their upstream value. They begin to increase well after the peak acceleration, and also after the rise of the streamwise ones. Near the wall, on the other hand, we observe a significant decrease (by over one order of magnitude) of the wall-normal Reynolds stresses (consistent with the observations of Blackwelder and Kovasznay¹¹) which is reflected in a similar decrease of the Reynolds shear stress $\langle u'v' \rangle / U_o^2$ (Figure 8(d)) in the buffer layer and in the viscous sublayer. In the logarithmic region, on the other hand, the increase in the streamwise fluctuation level balances the decrease of the wall-normal ones, resulting in constant shear stress until the recovery region (we will show later that the correlation coefficient does not vary very much in this region). Note that the data showed in this figure were normalized using the inflow freestream velocity, U_o , to emphasize advection effects. If one used either the local freestream velocity, U_∞ , or the friction velocity u_τ , which increase through the acceleration region, all these quantities would be observed to decrease through the region in which the pressure gradient is applied.

Figure 9 shows the structure parameter $a_1 = |\langle u'v' \rangle| / \langle u'_i u'_i \rangle$ and the correlation coefficient C_{uv} . The structure parameter is a measure of the efficiency of turbulence in extracting Reynolds shear stress from the

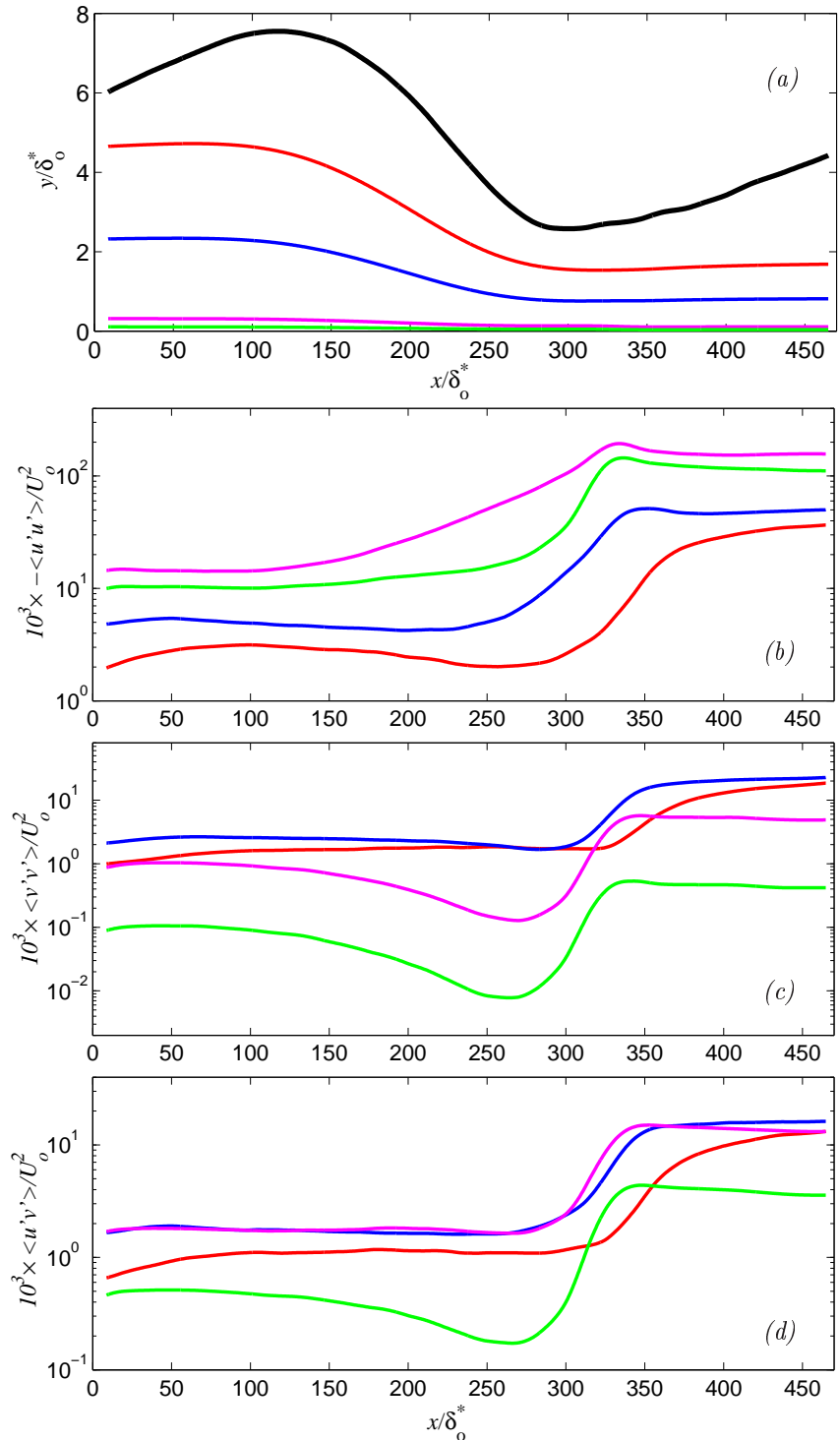


Figure 8. Development of the Reynolds stresses along selected streamlines. (a) Streamline coordinates; (b) $\langle u'u' \rangle / U_0^2$; (c) $\langle v'v' \rangle / U_0^2$; (d) $\langle u'v' \rangle / U_0^2$. The thick line corresponds to the boundary-layer edge. Streamline originating in: — outer-layer; — middle of the boundary layer; — logarithmic region; — viscous sublayer.

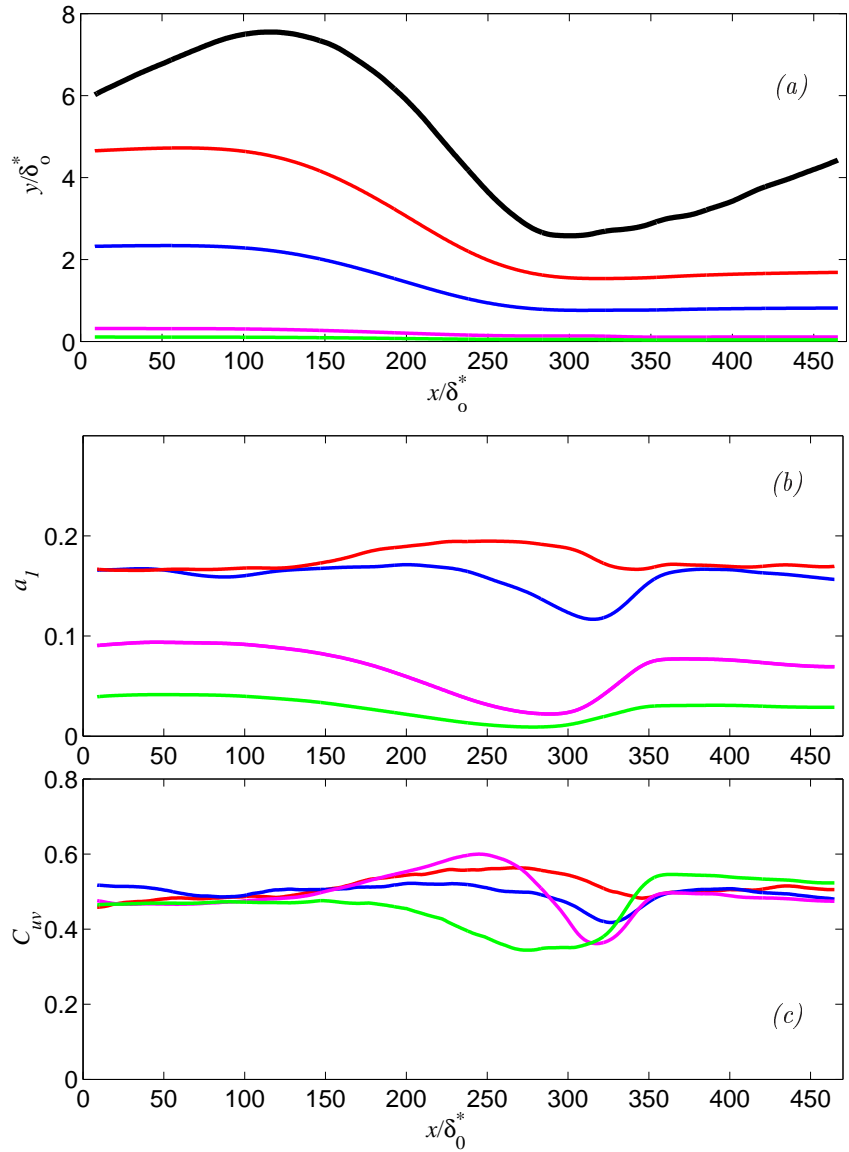


Figure 9. Development of a_1 parameter and correlation coefficient along selected streamlines. (a) Streamline coordinates; (b) a_1 ; (c) C_{uv} . The thick line corresponds to the boundary-layer edge. Streamline originating in: — outer-layer; — middle of the boundary layer; — logarithmic region; — viscous sublayer.

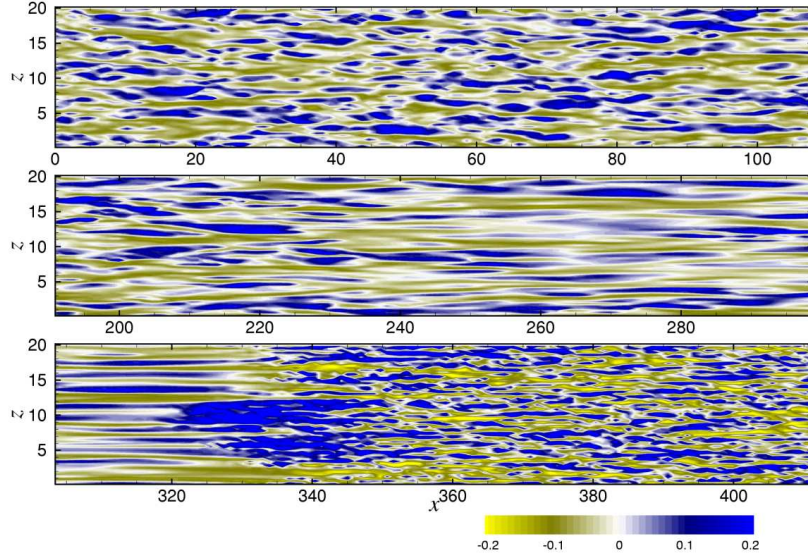


Figure 10. Instantaneous contours of u' velocity fluctuations in a plane parallel to the wall.

available turbulent kinetic energy and, in equilibrium flows, it has a value close to 0.15. The acceleration causes a significant departure from its equilibrium value: we observe a significant decrease of a_1 over the lower half of the boundary layer. The decrease is particularly strong in the logarithmic layer (the value of a_1 is lower in this region even in equilibrium ZPG boundary layers). The correlation coefficient C_{uv} , on the other hand, remains close to the canonical value for flat-plate boundary layers ($C_{uv} \simeq 0.4 - 0.5$) everywhere, with variations of less than 10%. Thus, the relaminarization does not seem to be due to so much to a decorrelation between the frozen fluctuations, but rather to a re-organization of the flow that results in much lower wall-normal fluctuations that, although reasonably well-correlated with the streamwise ones, can only produce a much reduced shear stress. The decreased mixing due to the turbulent transport, in turn, causes the decrease of the skin-friction coefficient that is considered one of the symptoms of relaminarization.

The significant changes to the turbulent statistics observe above must be accompanied by similar alterations of the turbulent structure, which we will now describe. The contours of streamwise velocity fluctuations in an xz -plane near the wall are shown in Figure 10. We can observe the regular streaky structure of the boundary layer near the inflow. In the region of high K we observe fluctuations of magnitude comparable to those in the equilibrium region; they form, however, very long streamwise streaks, without the kinks characteristic of the burst event. This indicates the change towards a very stable and more orderly inner layer, as pointed out by Narasimha and Sreenivasan.² Figure 10 also shows a fast re-transition to turbulence when the pressure gradient is turned off ($x/\delta_o^* \simeq 310$).

In Figure 11 the coherent structures in the outer layer are visualized through isosurfaces of the second invariant of the velocity gradient tensor

$$Q = -\frac{1}{2} \left(\frac{\partial u'_i}{\partial x_j} \frac{\partial u'_j}{\partial x_i} \right) \quad (7)$$

(see Dubief and Delcayre²⁷). We note that the outer layer vortices become aligned in the streamwise direction in the acceleration region. This is most likely a kinematic effect, as the dominant component of the velocity gradient in this region, $\partial U/\partial x$, has the effect of stretching and re-orienting the coherent eddies into the streamwise direction. We note, however, that the more orderly structure of the flow observed in the inner layer (Figure 10) is reflected in a more orderly outer layer structure. An obvious question that needs to be addressed is whether the inner layer, with its reduced burst frequency, is unable to “scramble” the outer layer structures, or if the outer layer forces a more orderly inner-layer structure. The outer layer structures certainly affect the inner layer: Figure 12 shows contours of the instantaneous $u'v'$ correlation in planes normal to the mean flow, and secondary ($v - w$) velocity vectors. One can observe several features of this

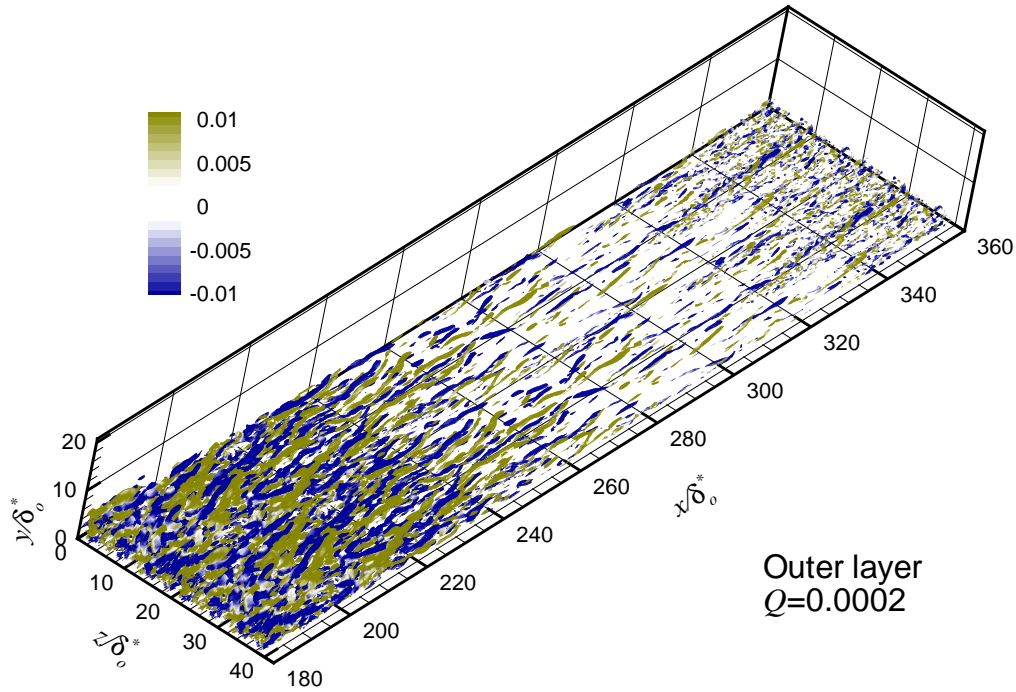


Figure 11. Instantaneous isosurfaces of $Q = -0.002$ in the outer layer colored by the streamwise vorticity.

flow field. First of all, these vortices occur mostly in the well-mixed region mentioned above (the two thick lines that denote contours of $\bar{u} = 0.95U_\infty$ and $0.99U_\infty$ show the extent of this well-mixed region); they may, in fact, be responsible for it, as they induce vigorous motions of high-speed fluid towards the wall, and low-speed fluid outwards. Moreover, some of the motions induced by these large vortices result in significant values of the $u'v'$ correlation (at $x/\delta_o^* = 321$ and $z/\delta_o^* = 11$, or at $x/\delta_o^* = 260$ and $z/\delta_o^* = 4$, for instance).

IV. Conclusions

We performed LES of the flow in an accelerating boundary layer, using two different levels of acceleration. The low-acceleration case remains in quasi-equilibrium, with a logarithmic law observed through most of the flow (albeit with decreased slope). The high-acceleration case results in relaminarization and re-transition of the flow. The computed statistics are in good agreement with the experimental data,¹⁴ which gives us confidence that the LES can be used to study the physics of this complex flow.

Examining the flow development along streamlines we observe that in the outer layer the turbulent fluctuations appear to be largely frozen to their initial state, and the flow is dominated by advection. A notable feature of the flow is that the correlation coefficient C_{uv} does not decrease very significantly. The decrease of the Reynolds shear stresses that is observed is mostly due to the damping of the wall-normal fluctuations.

We observed changes in the turbulent structures both in the inner and in the outer layers. The acceleration affects the outer-layer eddies by changing their structure and shape; in particular, large coherent structures are formed that are oriented in the streamwise direction. This results in the formation of a well-mixed layer, in which the turbulence production is decreased, and the turbulence advected from upstream remains frozen. The inner layer is also affected: because of the strong acceleration, the flow becomes more orderly, with longer, more two-dimensional streaky structures and decreased frequency of bursts. However, a fast re-transition to turbulence is observed as soon as the applied pressure gradient is negligible. This may be due to the coherent structures in the outer part of the flow that trigger the re-transition to turbulence.

Two possible scenarios can explain the flow behavior: one, which matches the results of Blackwelder,¹¹ Launder,^{7,8} Narasimha and Sreenivasan,² and Sreenivasan,¹ is that the inner layer is made stable by the pressure gradient, and the turbulence in the outer layer remains relatively high and “frozen”: once the

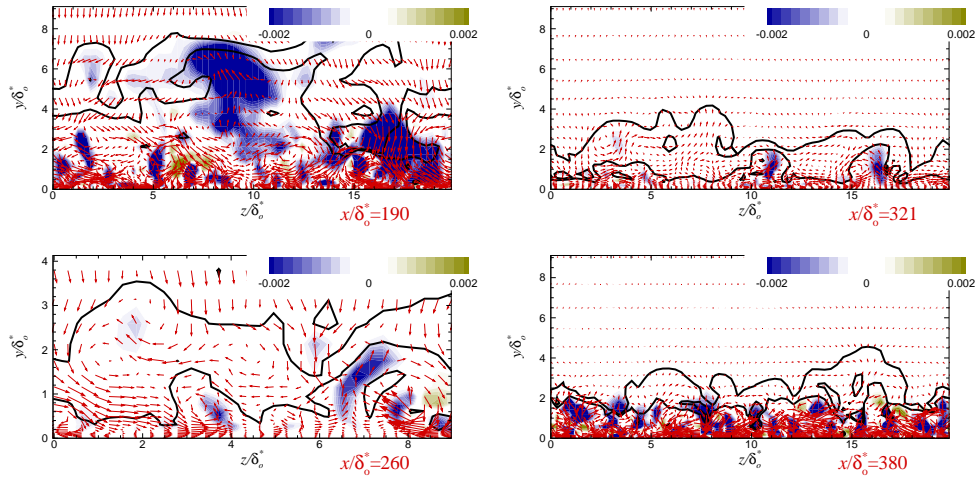


Figure 12. Contours of instantaneous $u'v'$ correlation in planes normal to the mean flow, and secondary ($v-w$) velocity vectors. The two solid lines represent contours of $U/U_\infty = 0.95$ and 0.99 .

stabilizing influence of the pressure gradient is removed, transition occurs very rapidly, following a process that resembles bypass transition due to high freestream turbulence. A different picture was conjectured by Falco¹² and later by Ichimiya *et al.*:¹³ the relaminarization seems to begin from the outer region with a strong coupling between inner and outer parts. The outer layer structures could induce strong incursions of more quiescent, outer-layer fluid into the wall region, and strong ejections of inner-layer fluid into the outer flow. Our data show that both of these mechanisms are present. Additional work is required to determine which of them is dominating.

Acknowledgments

Effort sponsored by the Air Force Office of Scientific Research, Air Force Materiel Command, USAF, under grant number F49620-03-1-0112, monitored by Dr. T. Beutner and Lt. Col. R. Jefferies. The US Government is authorized to reproduce and distribute reprints for Governmental purposes notwithstanding any copyright notation thereon. The views and conclusions contained herein are those of the authors and should not be interpreted as necessarily representing the official policies or endorsements, either expressed or implied, of the Air Force Office of Scientific Research or the US Government.

References

- ¹Sreenivasan, K.R. (1982) Laminarizing, Relaminarizing and Retransitional Flows. *Acta Mech.* **44**, pp.1-48.
- ²Narasimha, R. and Sreenivasan, K.R. (1973) Relaminarization in highly accelerated turbulent boundary layers. *J. Fluid Mech.* **61**, pp.417-447.
- ³Narasimha, R. and Sreenivasan, K.R. (1979) Relaminarization of Fluid Flows. *Adv. Appl. Mech.* **19**, pp.221-309.
- ⁴Wilson, D. (1954) Convective heat transfer to gas turbine blades. *Proc. Inst. Mech. Eng.*
- ⁵Patel, V. and Head, M. (1968) Reversion of turbulent to laminar flow. *J. Fluid Mech.* **34**, pp 371-392
- ⁶Senoo, Y. (1972) The boundary layer on the end wall of a turbine nozzle cascade. *Transaction of the ASME. MIT Gas Turbine Laboratory.* **35**, pp 1711-1720
- ⁷Launder, B.E., (1963) The Turbulent Boundary Layer in a Strongly Negative Pressure Gradient Gas. *MIT Gas Turbine Laboratory Report* **71**, pp. 1-28
- ⁸Launder, B.E., (1964) Laminarisation of the Turbulent Boundary Layer by Acceleration. *MIT Gas Turbine Laboratory Report* **77**, pp. 1-50
- ⁹Badri Narayanan, M., Rajagopalan, S. and Narasimha, R. (1977) Experiment on the fine structure of turbulence. *J. Fluid Mech.* **80**, pp. 237-257.
- ¹⁰Kline, S., Reynolds, W., Schraub, F. and Runstadler, P. (1967) The structure of turbulent boundary layers. *J. Fluid Mech.* **30**, pp. 741-773.
- ¹¹Blackwelder, R.F. and Kovaszny, L.S.G. (1972) Large-scale motion of a turbulent boundary layer during relaminarization *J. Fluid Mech.* **53**, pp. 61-83
- ¹²Falco, R.E. (1980) Combined simultaneous flow visualization/hot-wire anemometry for the study of turbulent flows *J. Fluids Eng.* **102**, pp. 174-182

- ¹³Ichimiya, M., Nakamura, I., and Yamashita, S. (1998) Properties of a relaminarizing turbulent boundary layer under a favorable pressure gradient *Exp. Thermal Fluid Sci.* **17**, pp. 37–48
- ¹⁴Fernholz, H.H. and Warnack, D. (1998) The effects of a favourable pressure gradient and of the Reynolds number on an incompressible axisymmetric turbulent boundary layer. Part 1. The turbulent boundary layer. *J. Fluid Mech.* **359**, pp. 329–356.
- ¹⁵Warnack, D. and Fernholz, H.H. (1998) The effects of a favourable pressure gradient and of the Reynolds number on an incompressible axisymmetric turbulent boundary layer. Part 2. The boundary layer with relaminarization. *J. Fluid Mech.* **359**, pp. 357–381.
- ¹⁶Escudier, M.P., Abdel-Hameed, A., Johnson, M.W. and Sutcliffe, C.J. (1998) Laminarisation and re-transition of a turbulent boundary layer subjected to favourable pressure gradient. *Exp. Fluids* **25**, pp. 491–502.
- ¹⁷Spalart, P. R. (1986) Numerical study of sink-flow boundary layers. *J. Fluid Mech.* **172**, pp. 307–328.
- ¹⁸Piomelli, U., Balaras, E., & Pascarelli, A. (2000) Turbulent structures in accelerating boundary layers. *J. Turbulence* **1** (001) pp. 1–16.
- ¹⁹Germano, M., Piomelli, U., Moin, P. and Cabot W. H. (1991) A dynamic subgrid-scale eddy viscosity model. *Phys. Fluids A* **3**, pp. 1760–1765.
- ²⁰Lilly, D. K. (1992) A proposed modification of the Germano subgrid-scale closure method. *Phys. Fluids A* **4**, pp. 633–635.
- ²¹Meneveau, C., Lund, T. S., and Cabot, W. H. (1996) A Lagrangian dynamic subgrid-scale model of turbulence. *J. Fluid Mech.* **319** pp. 353–385.
- ²²Lund, T. S., Wu, X., and Squires, K. D. (1998) Generation of turbulent inflow data for spatially-developing boundary layer simulations, *J. Comput. Phys.* **140**, pp. 233–258.
- ²³Orlanski, I. (1976) Simple boundary condition for unbounded hyperbolic flows. *J. Comput. Phys.* **21**, pp. 251–269.
- ²⁴Chorin, A. J. (1968) Numerical solution of the Navier-Stokes equations. *Math. Comput.* **22**, pp. 745.
- ²⁵Kim, J. and Moin, P. (1985) Application of a fractional step method to incompressible Navier-Stokes equations. *J. Comput. Phys.* **59** pp. 308–323.
- ²⁶Schlichting, H. (1979) Boundary layer theory, McGraw Hill, New York.
- ²⁷Dubief, Y., and Delcayre, F. (2000) On coherent-vortex identification in turbulence. *Journal of Turbulence* **1**, 1-22.